Nanotoxicology (doi: 10.3109/17435390.2013.796534)

Principal Component and Causal Analysis of Structural and Acute *in vitro* Toxicity Data for Nanoparticles

XUE Z. WANG[1], YANG YANG[1], RUIFA Li[1], CATHERINE MCGUINNES[2], JANET ADAMSON[3], IAN L. MEGSON[3], KENNETH DONALDSON[2]

[1] Institute of Particle Science and Engineering, School of Process, Environmental and Materials Engineering, University of Leeds, Leeds LS2 9JT,UK

[2] Edinburgh Lung and the Environment Group Initiative, Colt Research Laboratories, Medical School, Edinburgh, Scotland EH16 4TJ, UK

[3] Free Radical Research Facility, Department of Diabetes & Cardiovascular Science, University of the Highlands & Islands, Inverness IV2 3JH, UK

***Correspondence author:** Professor Xue Z Wang

Chair in Intelligent Measurement and Control

Institute of Particle Science and Engineering

School of Process, Environmental and Materials Engineering

University of Leeds

Leeds LS2 9JT

Tel: 0113 343 2427

Fax: 0113 343 2405

Email: x.z.wang@leeds.ac.uk

Abstract

Structure toxicity relationship analysis was conducted using principal component analysis (PCA) for a panel of nanoparticles that included dry powders of oxides of titanium, zinc, cerium and silicon, dry powders of silvers, suspensions of polystyrene latex beads, and dry particles of carbon black, nanotubes and fullerene, as well as diesel exhaust particles. Acute *in vitro* toxicity was assessed by different measures of cell viability, apoptosis and necrosis, haemolytic effects and the impact on cell morphology, while structural properties were characterised by particle size and size distribution, surface area, morphology, metal content, reactivity, free radical generation and zeta potential. Different acute toxicity measures were processed using PCA that classified the particles and identified four materials with an acute toxicity profile: zinc oxide, polystyrene latex amine, nanotubes and nickel oxide. PCA and contribution plot analysis then focused on identifying the structural properties that could determine the acute cytotoxicity of these four materials. It was found that metal content was an explanatory variable for acute toxicity associated with zinc oxide and nickel oxide, whilst high aspect ratio appeared the most important feature in nanotubes. Particle charge was considered as a determinant for high toxicity of polystyrene latex amine.

Keywords: Nanoparticle toxicity, Structure-Activity Relationships Analysis, SAR, principal component analysis, nanoparticle characterisation

1. Introduction

Rapid developments in the manufacture and use of engineered nanoparticles (NPs) have also led to an urgent need for assessing their possible risk to humans and the environment (Lam et al. 2004; Thomas and Sayre 2005; Handy et al. 2008; Balshaw et al. 2005; Nel et al. 2006; Donaldson et al. 2004; Oberdorster et al. 2005c). Various NP toxicity testing methods have been studied, including general toxicity testing (Oberdorster et al. 2005a; Crane et al. 2008; Tsuji et al. 2006), assessment of toxicokinetics of NP in animal models and humans (Oberdorster et al. 2005c), as well as *in vitro* (Cui et al. 2005; Barlow et al. 2005; Shvedova et al. 2003) and *in vivo* (Lam et al. 2004; Muller et al. 2006) assays. Research has been conducted to assess the potential impact of particle size, size distribution, shape, surface area, state of dispersion and surface chemistry on toxicity (Powers et al. 2006; Handy et al. 2008; Powers et al. 2007; Murdock et al. 2008; Crane et al. 2008; Burello and Worth 2011b). The sheer number of potential NPs variants (different sizes and coatings, for instance) means that the only rational way of avoiding the necessity to test every single NP and its variants in toxicology tests, is to relate the physicochemical characteristics with their toxicity in a structure - activity relationship (SAR) model (Burello and Worth 2011a; Burello and Worth 2011b; Puzyn et al. 2011). The purpose of this study was to apply principal component analysis (PCA) for structure–toxicity link analysis for NPs. A panel of NPs that are in greatest bulk production and, therefore, present the greatest potential for environmental human exposure, was selected for the study. The NPs were subject to systematic characterisation of particle size and size distribution, surface area, morphology, metal content, reactivity, free radical generation and zeta potential. For the NPs in the panel, a range of tests were conducted to determine toxicity, haemolytic potential and the impact on cell morphology in acute toxicity cell culture models *in vitro*.

The eighteen NPs that constitute the panel are shown in Table 1. There are eight metal oxides of aluminium, cerium, nickel, silicon, zinc and titanium, silver metal (dry and in suspension), three polystyrene latex suspensions, and powders of carbon black and diesel particulate. Figure 1 shows SEM and TEM images of the samples.

2. Acute Cytotoxicity Assays and Structural Characterization of Nanoparticles

A wide range of assays are routinely used to assess acute cytotoxicity in cell culture; some allow assessment of the cell population that remains viable after a given treatment, whilst others assess markers the instigation of programmed cell death (apoptosis) and/or the ultimate necrosis that results from apoptosis or from other processes that ultimately cause death (e.g. mitochondrial poisoning, cell lysis). Given that each assay provides different information pertaining to the mechanism underpinning any acute cytotoxicity measured, a wide range of assays was selected for the current study in order to allow a comprehensive and comparative assessment of the assays in response to acute (24 h) exposure to the NP panel. In addition, different human cells (THP-1 monocytes, A549 lung epithelial cells and primary red blood cells) were assessed on account of both the applicability of the tests to specific cell types (e.g. adherent cells vs. cells in suspension) or their relevance to a specific test (e.g. haemolysis in red blood cells only).

2.1 Acute in-vitro cytotoxicity assays

Lactate Dehydrogenase Release Assay (LDH) is based on the concept that LDH is released into the supernatant by A549 epithelial cells once their membrane integrity is compromised – a characteristic of the late stages of cell death. The values generated are compared to those for an equivalent number of cells that have been treated with detergent (Triton X) to physically disrupt the membrane and cause 100% cell death. Figure 2(a) shows the results of the LDH release assay.

Apoptosis/Necrosis assays involving dual staining with annexin V, a cell-surface marker for apoptotic cells, and propidium iodide (PI), a DNA intercalating agent which only enters cells that have lost membrane integrity, were carried out using flow cytometry. This assay enables identification of apoptotic (annexin V positive), necrotic (PI positive) and viable (negative for both annexin V and PI) cells in a given cell population (figures 2(b), (c) and (d)).

Pro-Inflammatory effects were also analysed. A commercial ELISA (Active Motifs) was used to measure migration of NF-κB protein to the nucleus following two-hour exposure to each of the panel of NPs. The dose for most particles was 125 μg/ml, except nanotubes (N3), aminated beads (N6) and nickel oxide (N12), which were tested at a dose of 31.25 μg/ml. The results can be found in the Supplementary Materials,

Figure SM1(a). Only aminated polystyrene beads (N6) and zinc oxide (N14) induced a reduction in levels of P65 NF-κB protein in comparison to control.

Red blood cell haemolysis assays were conducted to determine the effect of different nanoparticles on membrane surface integrity. Erythrocytes were obtained from fresh human venous blood, following removal of plasma and buffy-coat layer after centrifugation. The washed erythrocytes were incubated with NaCl (negative control), 250μg/ml of nanoparticles and quartz - a known haemolytic particle) and Triton X (positive control; Sigma) for a period of 20 minutes. The subsequent percentage of haemolysis was determined by measuring the absorbance of the supernatant at λ=550nm. The results can be found from the Supplementary Materials, Figure SM1(b).

Cell viability was also assessed in A549 lung epithelial cells exposed to NPs (24 h; 1-100 μg/ml) in terms of mitochondrial function, using a commercially available assay **(MTT).** The basis of this assay viable cell-mediated conversion of colourless, water soluble (3-(4,5-dimethylthiazol-2-yl)-2,5-diphenyltetrazolium bromide; MTT) to an insoluble formazan that can be measured spectrophotometrically (λ=570 nm). Conversion of the formazan to MTT is dependent on NAD(P)H reductase enzymes, and hence is related to the metabolic activity of the cells.

The mitochondrial impact of the NP panel was explored in more detail using a flow cytometry-based assessment of mitochondrial membrane potential using the fluorescent dye, **DiOC6,** to detect collapse of this potential. Traditionally, this test is used as an early marker of apoptosis and is conducted in parallel with a test for secondary necrosis (PI in this case). This test was conducted in a different, but equally relevant, cell type (THP-1 human monocyte-like cells) because the assay is better-suited to non-adherent cells that remain in suspension.

MTT and DiOC6 assays were conducted on A549 and THP-1 cells respectively after treatment with NPs (10-100μg/ml; 24 h) in order to determine acute cytotoxicity in terms of mitochondrial function (the results can be found in the Supplementary Materials, Figure SM2(a)).

The majority of particles were found to be relatively non-toxic in A549 cells using the MTT assay (24 h exposure): only aminated beads (N6) and nanotubes (N3) showed toxic profiles in this assay. The DiOC6 measure of mitochondrial membrane potential indicated a slightly different activity profile, with diesel

exhaust particles (N2) showing a significant effect on mitochondrial membrane depolarisation (Supplementary Materials Figure SM2(b)). The apparent effect of polystrene latex beads (carboxylated; N7) in this assay might be due to the well-recognised autofluorescence of carboxylated latex beads, which could interfere with the assay. Nanotubes (N3) were the only other NP with substantial (>20%) effects in this assay, whilst aminated latex beads (N6) once again caused substantial necrosis. Interestingly, in the majority of cases where NPs induced a collapse of mitochondrial membrane potential, there was not a profound increase in PI-detected necrosis, which might have been expected in the wake of instigation of apoptosis. Whilst this disconnect between apoptosis and necrosis might simply be explained by insufficient time for necrosis to develop in this 24 h snapshot, it is tempting to speculate that these specific NPs might induce mitochondrial dysfunction that could be detrimental to human health without necessarily causing cell death.

It was noticed through the ***Cell Morphology Assay*** conducted in A549 cells that some of the NPs that failed to induce a toxic effect nevertheless changed the morphology of the cells in that they appeared to fail to spread over the substratum, but instead rounded-up and formed aggregates. As a result, a formal assessment of effect of nanoparticles on morphology was undertaken in an effort to identify those nanoparticles that induced a physiological effect without necessarily resulting in cell death (Supplementary Materials, Figure SM2(c)). The results indicate that the biggest effect was seen with aminated beads (N6), but a range of other NPs had detectable effects on cell morphology (N2, 3, 5, 7, 13, 15 and 16). The implication of this finding is that a number of NPs that fail to have substantial acute toxic effects, as measured by a range of other assays, might nevertheless have a potentially detrimental effect on cell function that could, ultimately, impact on health.

2.2 Characterization of structural properties

Particle shape for all samples was analysed using LEO 1530 Scanning Electron Microscope (SEM). Samples of aluminium oxide (N8), silicon oxide (N13) and titanium oxide anatase (N16) were also analysed using Philips CM20 Transmission Electron Microscope (TEM). The images for the 18 particles

given in Figure 1 were all SEM images. Two variables, the calculated aspect ratio and the mean particle size, were used in further SAR analysis.

Surface area and porosity were measured using TriStar 3000 BET. The instrument provides thirteen measurements, including five surface areas based on different definitions, three pore volumes, three pore sizes, as well as the mean size and particle density. Details of the thirteen attributes measured by TriStar 3000 are given in the Supplementary Materials, Table SM1. The analyser is based on gas adsorption and capillary condensation principles and uses different methods, including the BET theory (Brunauer et al. 1938), Langmuir method (Langmuir 1916) and BJH procedures (Barrett et al. 1951) to obtain information about the surface area and porosity of a solid material. BET measurements were obtained only for the14 dry powder samples, and could not be conducted for the four suspensions (N5, N6, N7 and N18).

Particle size and size distribution were analysed using a Malvern MasterSizer 2000. In addition to 100 attributes for size distribution, the MasterSizer also gives a list of seven other size properties, including the mass diameter, uniformity, specific surface area, surface area mean diameter and three mass diameters, as shown in the Supplementary Materials Table SM2. The sizes of nanoparticles can also be estimated from SEM/TEM images and the TriStar 3000 analyser. Results from these three different methods indicate that measurements from the TriStar 3000 and SEM/TEM imaging methods are very close, whilst those from the Mastersizer 2000 are much larger. This could be due to the fact that there is aggregation or agglomeration of the particles in the prepared suspensions.

Oxygen-centred free radical generation (electron paramagnetic resonance; EPR) was used to determine the oxygen-centred free radical generation from NP suspensions in the absence of any tissue interferences using DMPO and Tempone H as relatively selective spin-traps for hydroxyl and superoxide radicals respectively. It was found that carbon black (N1), diesel exhaust (N2), zinc oxide (N14), titanium dioxide anatase (N16) and nano-silver (N18) showed significant levels of superoxide radical generation. Zinc oxide (N14) and nano-silver (N18) also had significant hydroxyl radical generation.

In order to further test the ***particle reactivity in solution*** of the different NPs, the dithiothreitol (DTT) consumption test, using DTT as a reducing species, was carried out (Sauvain et al. 2008). Since the DTT

consumption test can only be conducted on dry powders, only fourteen of the panel of NPs were assessed using this assay.

All the carbonaceous NPs appeared to be able to catalyze the oxidation of DTT by O_2. Carbon black (N1) was the most reactive, followed by diesel exhaust particles (N2) and then nanotubes (N3). Fullerenes (N4) barely showed any activity. Diesel exhaust particles (N2) reactivity was rather small compared to published values (Sauvain et al. 2008; Geller et al. 2006). The low nanotube (N3) reactivity may be due to difficulties to produce a homogeneous suspension.

The DTT test has been reported to be non-responsive to inorganic species and metals (Cho et al. 2005). In general, the results correspond to the previous findings for inorganic species, but there are exceptions. Indeed, nickel oxide (N12) and silver metal (N17) present a significant reactivity towards DTT. A second interesting observation is that the non-reactive metal oxides were relatively non-reactive in the DTT consumption test: zinc oxide (N14) has the highest activity in this respect (-9 ± 2 pmol/min/μg). The values presented for some of the metals and metal oxides is due to subtraction of the blank and indicates that DTT oxidation in the absence of the NP is faster than in its presence (i.e. NPs like ZnO actively inhibit auto-oxidation of DTT).

Metal Concentration Metal concentration is one of the factors that are likely to be important in nanoparticle toxicity. For all these 18 nanoparticles, the concentrations of ten metals (Ti, V, Cr, Mn, Fe, Co, Ni, Cu, Zn and Cd) were measured, as shown in Table 2. Silver concentration was not measured, not only because it requires a very complicated procedure to perform the measurement, but also due to the fact that the dissolution is so slow as to not be important in our 24 h exposures (Kent and Vikesland 2012). These ten are metal ions measured in water, representing the metals on the surface of the NPs. Samples were digested for ICP-MS analysis using a CEM MDS-200 microwave system. Particle samples were washed into Teflon-coated composite vessels using 5 ml of 70% nitric acid. The samples were digested using an existing program developed for refractory carbon-based particle matter (Jones et al. 2006; Price et al. 2010). The microwave program consisted of a stepped increase in pressure to 80 psi for a period of 20 min, with a corresponding temperature rise to 180ºC. The program lasted for approximately 2.5 h, including warm-up and cool-down periods. Samples were then diluted to a level of 10 μg/ml (dependent upon their original weight) using deionized (>18 ΩM) H_2O. Raw data were corrected for blanks and controls accordingly.

3. Principal Component Analysis of the Cytotoxicity Data

3.1 Principal Component Analysis (PCA)

PCA is an established methodology well documented in text books. Briefly, the technique uses a linear mathematical algorithm to derive a new set of variables, called principal components (PCs), from the original variables in such a way that the new set of variables are no longer correlated. Via a method called contribution plot analysis, PCA can also highlight those original variables amongst the data that contribute most to the variance in the original data. By then focusing on these "principal components" the data can be re-analysed to assess whether certain combinations of key variables account for differences between, in our case, test NPs. For example, should all the NPs that were most toxic display a consistent combination of physical characteristics, they would appear as a discrete cluster in PCA, distant from those that were non-toxic.

Every PC is the linear addition of the original variables. The principal components are also called *scores*, while the weight that quantifies the linear contribution of each original variable to a PC is often known as *loading*. It can be interesting to find the relative contribution of the original variables to a specific principal component. This can be analyzed by plotting the loadings. Since the original variables are scaled before PCA is applied, the larger the loading, the more contribution that original variable makes.

Instead of developing a mathematical model that quantitatively predicts the toxicity end-points using the structural and compositional descriptors measured in section 2.2 as the inputs, the SAR analysis in this work has focused on identifying the descriptors that are responsible for the observed high toxicity values of NPs from the panel. In this model, the metal contents are called compositional descriptors, and all the remaining parameters, including size, size distribution, morphology, surface area, reactivity, are called structural descriptors. When we mention physico-chemical descriptors we mean the two types of descriptors combined.

PCA was applied to process the structural and compositional descriptors of the samples in order to remove the correlations between the descriptors and reduce dimensionality. The obtained PCs were then used for clustering and link analysis. The hypothesis was that the particle samples that show high toxicity would be

distinguished as a cluster, based on the structural and compositional descriptors. The descriptors underlying clustering can then be identified as those responsible for the observed toxicity.

In all PCA analysis in this work, the original data were scaled before PCA analysis. This was carried out in two steps: first, mean centring, i.e. subtracting the mean of the data; and second, range scaling to between 0 and 1, using the minimum and maximum of the data. This operation was carried out for each attribute of the structural properties separately. For the ten metal and metal oxide NPS, the scaling operation was performed together.

3.2 *PCA Analysis of Cytotoxicity Data*

As indicated in Figure 2, the acute cytotoxicity of NPs is generally dose-related. The best approximation of toxicity of a given NP is provided by a summary of toxicity across the range of concentrations measured, as opposed to at a single point. PCA is a useful tool to aggregate the values together so one can use a single value (or two values) to describe a curve. In this study, we put all the data from different acute toxicity measures together, including those presented in Figure 2, the pro-inflammation effects, haemolysis, MTT cell viability assay and $DiOC_6$ mitochondrial membrane potential data, and processed the data using PCA. This operation not only reduced the data dimension, but took account of the likelihood of parallels between different cytotoxicity measures. It was found that the first three principal components, PC1, PC2 and PC3, captured 76%, 20% and 1% of the variance respectively. As reviewed by Valle et al (Valle et al. 1999), various approaches exist for determining how many PC*s* should be retained. One of the suggested methods is to plot the variance captured by every PC and examine the trend. In our case, since PC1 and PC2 together captured 96% of the variance, and there is a sharp reduction in captured variance to PC3, only two PCs were considered necessary in this case. The PC1-PC2 plot in Figure 3 clearly shows that aminated beads (N6), zinc oxide (N14), nanotubes (N3) and nickel oxide (N12) are separate from the remainder of the NPs, which appear as a cluster. Examination of this cluster indicates that it contains the low acute toxicity particles. Aminated beads (N6) have the highest acute toxicity values in nearly all assay results (LDH, apoptosis, necrosis, haemolytic, MTT and cell morphology assays). Zinc oxide (N14) has a high acute toxicity value in LDH, apoptosis, necrosis and inflammation assays. Nanotubes (N3) have high acute toxicity values in viability and MTT assays. Nickel oxide (N12) has high acute toxicity as measured by the LDH and haemolytic assays.

PCA and clustering were then applied to process the physicochemical descriptors with the hypothesis that the NPs with acute toxicity might also be discriminated from the non-toxic NPs based on the analysis of the measured physicochemical descriptors. Should this be the case, further analysis can be conducted to identify the key physicochemical descriptors that lead to the observed acute toxicity. Since, for the four samples in suspension, (N5, N6 and N7 and N18), no BET or DTT data is available, PCA analysis was carried out in two different ways. Firstly, all the 18 samples were analysed without including BET or DTT measurements. Secondly the 14 dry samples were analysed together with the BET and DTT attributes included. Both results are presented.

4. PCA Analysis of Structural Data and Structure-toxicity Causal Analysis

Having observed above (Figure 4) that PCA analysis of acute cytotoxicity data clearly grouped the NPs with low acute toxicity into a single cluster, and singled-out the NPs with high acute toxicity, we went on to test the possibility that PCA analysis of the structural data alone (excluding toxicity data) would group the data in a similar way, implying that it was the structural difference that was associated with the level of acute toxicity displayed. In addition, we studied the use of a PCA contribution plot technique to pinpoint to the structural descriptors that are responsible for the observed high toxicity values.

4.1 PCA analysis of the physicochemical descriptors of the 18 samples, excluding BET and DTT data

PCA analysis of the physicochemical properties of the 18 samples, excluding BET and DTT data because the four wet samples (three polystyrene latex suspensions N5, N6 and N7 as well as silver suspension N18) do not have BET and DTT data, shows that the first three PCs captured variations of 42%, 31% and 14% respectively. The first three principal components were selected to represent the original high dimensional dataset, since including the 4^{th} PC gives the same result. Figure 4 is the PC1-PC2-PC3 three-dimensional plot showing that the 18 nanoparticles were clearly grouped into clusters. The clustering result based on visual inspection of the plot is the same as that obtained by applying a clustering technique, k-means, using the three PCs; therefore, the k-means result is not presented here. The largest cluster contains NPs (red circles) that showed low acute toxicity. However, nanotubes (N3), nickel oxide (N12), zinc oxide (N14) and diesel exhaust particles (N2) clearly are outside this low acute toxicity sample cluster.

As previously noted in the chemometric analysis of the acute toxicity data, nanotubes (N3) and nickel oxide (N12) are highly toxic. Diesel exhaust particles (N2) did not feature as having high acute toxicity from the PCA analysis of toxicity data and so separate examination of this NP is merited and will be made later.

It is also interesting to note that aminated beads (N6), one of the samples that showed high acute toxicity, was not assigned to the largest cluster that contains the non-toxic samples, but grouped closely with the other two polystyrene latex beads, unmodified beads (N5) and carboxylated beads (N7), which showed no acute toxicity. Therefore, it was suspected that there must be another reason, or reasons, that led to the high acute toxicity displayed by N6 that was not shared by N5 and N7; this will be examined later.

To examine the clustering results more closely, two-dimensional plots of PC1-PC2, PC1-PC3 and PC2-PC3 were also studied (plots not shown). Examination of these three two dimensional plots revealed that it is PC2 that separated nanotubes (N3) from the other samples, and that N3 cannot be segmented from the other samples in the PC1 and PC3 plot. The next step was to identify the link between the main original variables that contributed to the discrimination of nanotubes (N3) from the remaining NP samples. This can be done via contribution plots of the loadings, i.e. coefficients of the original variables against the principal component. This treatment of the data gave information of the relative contribution for each original variable made to a latent variable, a PC. The contribution plots for PC1, PC2 and PC3 are shown in Figure 5, although we are mainly interested in the contribution to PC2 (solid red colour), since it is PC2 that discriminated nanotubes (N3) from the other NP samples. It can be seen that the original variables that made the largest contributions to PC2 are: aspect ratio, measured by SEM imaging, and volume, weighted mean, uniformity, and D(0.9), all measured by Mastersizer, as well as Ni and Zn metal contents. It was also noticed from the PC1-PC2, PC1-PC3 and PC2-PC3 plots that it is again PC2 that led to the discrimination of nickel oxide (N12) and zinc oxide (N14) from the main, non-toxic sample cluster. From the contribution plot analysis, it is clear that it is not conclusive whether all of these important variables are responsible for the high acute toxicity of nanotubes (N3), nickel oxide (N12) and zinc oxide (N14), or only a few of them. Furthermore, it is unclear which original variables are responsible for the toxicity of each particular NP. Further analysis is therefore required - PCA should not be considered to be a means to provide a complete answer, instead it should be seen as a tool for disentangling complex data to the extent to be able to generate new hypotheses for subsequent testing.

Before performing further analysis to narrow down on those attributes that contributed to the high acute toxicity of N3, N12 and N14, it is necessary to assess if the inclusion of BET and DTT data in PCA analysis could lead to different results. Therefore, PCA analysis of the 14 dry nanoparticles was performed, and compared with the results obtained above.

4.2 PCA analysis of the 14 dry samples to include the BET and DTT data

In order to include the BET and DTT data, the structural and compositional descriptors for the 14 powders (excluding the three polystrene latex beads, N5, N6 and N7 and silver suspension (N18) were then processed using PCA. The PC1-PC2-PC3 plot is given in Figure 6. It also shows that nanotubes (N3), nickel oxide (N12), zinc oxide (N14), and diesel exhaust particles (N2) are isolated from the cluster containing the non-toxic NPs. PC1-PC2, PC1-PC3 and PC2-PC3 two dimensional plots (not shown here) were also examined with very similar outcomes. In this case, it was PC3 that distinguished nanotubes (N3) from the rest, and PC2 distinguished nickel oxide (N12) and zinc oxide (N14) from the rest (although diesel particles (N2) were always close to N12 on this occasion). It is important to note that PC3 here does not correspond with the PC3 when data for the 18 nanoparticle samples that were analysed used PCA. Contribution plot analysis found that the variables that made the most substantial contributions to PC3 are aspect ratio (from SEM image analysis) and volume weighted mean, uniformity and D (0.9) from Mastersizer, suggesting that they are the core variables that explain the high acute toxicity value of nanotubes (N3). The Ni and Zn contents made little contribution to PC3, implying they are not the reasons of high acute toxicity value for N3. Contribution plot analysis for PC2 found that the main variables are Ni and Zn content, as well as D(0.1), D(0.5) measured by Mastersizer and SPSA measured by TriStar 3000 BET, suggesting that these might be the key variables responsible for high acute toxicity of N12 and N14. Therefore, for the 14 dry particles, PCA analysis with the BET and DTT data included, gives similar results to analysis in which BET and DTT were excluded in the analysis for the 18 particle samples.

4.3 PCA analysis of the structural properties only, excluding metal contents

In order to determine exactly which physicochemical attributes lead to high toxicity values of nanotubes (N3), nickel oxide (N12) and zinc oxide (N14), PCA analysis of the structural data alone, without including metal contents, and also PCA analysis of metal contents alone, without considering structural descriptors,

were also performed, and the results analyzed. Three PCs were also selected from PCA analysis of the 18 samples of the structural descriptors only (excluding BET and DTT attributes, and metal contents). Figure 7 is the 3D plot of PC1-PC2-PC3 that shows nanotubes (N3) were separated from other low acute toxicity samples due to PC2, while the three polystyrene beads (N5, N6 and N7) were in an isolated group. However, nickel oxide (N12) and zinc oxide (N14) were grouped with non-toxic materials. It indicates that it is very unlikely that the structural descriptors have led to high acute toxicity values for N12 and N14. PC1-PC2, PC1-PC3 and PC2-PC3 plots (not shown) confirmed the observation made above. The contribution plot for PC2 reveals that aspect ratio, volume weighted mean, uniformity, and D(0.9) are the main variables, suggesting that they are likely the responsible variables. In fact, as will be seen next in PCA processing of the metal contents only, nanotubes (N3) cannot be distinguished from the rest of the panel based on metal content, implying that metal content is not responsible for high acute toxicity of N3. PCA analysis of the structural properties, including BET and DTT, for 14 samples was also performed. The result (data not shown) was consistent with those from the above analysis for the 18 samples, i.e. nickel oxide (N12) and zinc oxide (N14) cannot be discriminated, but that nanotubes (N3) were separated, and contribution plot analysis points to the same original variables, i.e. aspect ratio, volume weighted mean, uniformity, and D(0.9). PCA analysis of BET data alone was also performed. No meaningful clustering was observed, suggesting that BET-measured descriptors did not play a key role in discriminating the samples.

4.4 PCA analysis of the metal contents only, excluding structural descriptors

The soluble metal concentration of each NP is shown in Table 2. PCA was applied to the compositional descriptors of the samples in order to find out whether metal components are associated with acute toxicity. PCA analysis found that the first and second principal components captured variations of 79.9% and 20% respectively. Figure 8 is the PC-PC2 plot of compositional descriptors for 18 samples. It shows that most samples gather in one group: nickel oxide (N12) is an exception separated on account of PC1, whilst zinc oxide (N14) and diesel exhaust particulate (N2) were both separated on account of PC2. To identify the relative contribution of each metal to PC1 and PC2, the contribution plots to PC1 and PC2 revealed clearly that Ni content made the most important contribution to PC1, while Zn content made the most noticeable contribution to PC2. The result suggests that Ni content may be the main reason for the high acute toxicity

for nickel oxide (N12) and zinc content may be the reason for diesel exhaust particles (N2) and zinc oxide (N14). Examination of Table 2 indicates that nickel oxide (N12) is the particle with the highest Ni content, while zinc oxide (N14) and diesel exhaust particles (N2) are both high in Zn. Similar plots for other metal contents (not shown) cannot distinguish N12, N14 and N2.

4.5 Identifying the factor that discriminates N6 (polystrene latex amine) from N5 (unmodified) and N7 (carboxylated)

With regard to the three polystyrene latex samples (unmodified - N5, aminated - N6, and carboxylated - N7), the above PCA analysis results are summarised as follows: firstly, PCA analysis of metal contents only (Figure 8) could not discriminate N5, N6 and N7 from the largest clusters of non-toxic particle samples. Secondly, PCA analysis of structural descriptors only, as well as PCA analysis of both structural and compositional descriptors together, all indicates that N5, N6 and N7 are grouped in the same cluster, separated from other particle samples, indicating they are distinct from other nanoparticles as far as structural descriptors are concerned. However, the fact that they are grouped together is an indication that they are very similar in structure; it is unlikely that structural descriptors contributed to the toxicity of N6, given that N5 and N7 are not toxic in the acute setting.

The data to this point therefore suggested that physico-chemical properties not yet analysed might represent the cause of the specific acute toxicity of the aminated latex beads. Given the similarity of the beads in all aspects measured to date, our focus shifted to the amine group itself as the source of the acute toxicity, either on account of the charge differential or via a chemical effect mediated by amine groups. As a result, zeta potential was measured for all three polystyrene latex samples, using Malvern Instrument's Zetasizer Nano instrument. For each sample, three measurements were taken. The measured zeta potentials (mV) for the amine polystyrene (N6) are 37.8, 37.5, and 40.3, for *unmodified (N5) are -36.2, -38.8 and -36.8, and for carboxylated (N7) are -54.9, -55.3, and -58.6. N6 has a positive zeta potential value, while N5 and N7 have negative zeta potentials. According to the literature (Arvizo et al. 2010a; Arvizo et al. 2010b; Nel et al. 2009; Verma et al. 2008; Rivera-Gil et al. 2012), any particle with positive charge is likely to interact electrostatically with cells because most cell membranes are negatively charged under physiological resting

conditions. Therefore, it is possible that the large positive charge of N6 is at least partly responsible for its high acute toxicity, despite it structurally similar to N5 and N7.

4.6 Diesel exhaust particles (N2)

In PCA analysis of the acute toxicity data (Figure 3), diesel exhaust particles (N2) were found amongst the largest cluster of NPs with low acute toxicity. N2 deserves special attention because, unlike other nanoparticles in the low toxicity cluster of Figure 3, PCA analysis of the physicochemical (both structural and compositional) descriptors (Figure 6) and of the compositional (metal content) only (Figure 8), indicated that N2 is always discriminated from other particles of the low acute toxicity particle cluster of Figure 3. N2 was not discriminated from the PCA analysis of the structural descriptors alone (Figure 7), suggesting that it does not appear to be structural difference that causes N2 to be different from the low toxicity NPs. PCA analysis of metal contents only (Figure 8) shows that N2 is clearly discriminated from other nanoparticles, and it is PC2, and not PC1, that is central to the separation. The contribution plot for PC2 shows that zinc content made the most important contribution. Zinc content of all NPs can also be seen from Table 2, which shows that N2 (diesel exhaust) has the second largest zinc content. The largest zinc content was attributed to N14 (zinc oxide), 2.6 times higher than N3, and showed high toxicity, as has been analysed earlier.

Diesel exhaust particles (N2) seemed to be non-toxic, based on the PCA analysis of acute toxicity measures (Figure 3). If we look at individual acute toxicity measurements, most did not suggest high acute toxicity for N2. The exception is its high impact on mitochondrial membrane potential ($DiOC_6$). Given the combined results presented in this study, the assumption that mitochondrial membrane potential collapse always precedes apoptosis does not appear to be the case in this instance because secondary necrosis does not seem to follow. The suggestion from our results is that diesel particulate has a property that prompts mitochondrial membrane collapse without necessarily inducing apoptosis. The functional significance of the finding is not yet fully understood, but further research is underway to investigate this issue.

5 Discussion

SAR analysis generates the following conclusions. The most likely cause of high acute toxicity for nanotube (N3) is its shape (high aspect ratio). Length is an important parameter for fibre toxicity, as described in the fibre pathogenicity paradigm (Donaldson et al. 2010), which is relevant to carbon nanotubes (Murphy et al.; Poland et al. 2008). Our previous studies with the same carbon nanotubes have suggested that they are long enough to cause frustrated phagocytosis (Poland et al. 2008). Studies with nickel oxide nanowires (Poland et al.) and silver nanowires support the contention that nanofibre length is likely to be a factor leading to inflammogenicity and toxicity. The analysis attributes the high acute toxicity of zinc oxide (N14) and nickel oxide (N12) to their high contents of zinc and nickel. It is well documented that the soluble ions derived from zinc oxide NP play a role in cellular toxicity of this nanomaterial (Cho et al. 2012) as a consequence of dissolution inside lysosomes (Nel et al. 2009). In contrast to the conclusion reached here, soluble nickel ions from the same nickel oxide NP, were not found to have any toxic effects on cells in culture, nor did these aqueous extracts have the ability to induce inflammation when instilled into the lungs of rats (Cho et al. 2012) However, nickel oxide NP are highly acidic in solution and we believe that the acid-released Ni ions would be a truer reflection of the effective dose of Ni ions than the saline (basic)–released nickel ions.

Polystrene latex amine (N6) was found to always be in the same cluster as the other two non-toxic polystrene latex beads, unmodified (N5) and carboxylated (N7). This prompted us to measure the zeta potential of the three polystrene latex beads. The result suggests that the high positive charge of N6 could be associated, at least in part, with its high toxicity. N5 and N7 showed high negative charge. The surface charge of NP, measured by zeta potential has been suggested to be an important factor in the ability to cause cellular injury. Nel et al (Nel et al. 2009) described high positive zeta potential of particles as a factor in destabilising the phagolysosome after uptake. The positive zeta potential on NP is immediately neutralised on formation of a corona after deposition in lung lining fluid, but inside the lysosomes the acidity combined with the protease/lipase activity may be able to remove this corona, revealing the charged surface. The naked particle would then be free to interact with the lysosomsal membrane, leading to rupture and release of lysosomal contents with concomitant activation of the NALP3 inflammasome, as has been shown for quartz particles (Hornung et al. 2008). Another hypothetical mechanism whereby positively charged NP might destabilise membranes implicates accumulation of chloride ions and water as a consequence of chronic stimulation of the lysosomal membrane proton pump (Nel et al. 2009).

Some other cautious observations were also made which might only be relevant for the specific NPs tested in this particular panel. Although the literature suggests that surface area is a major factor in determining NP toxicity, this association was not confirmed in our study. Indeed, chemometric analysis of the BET data only for the fourteen dry samples, did not find a meaningful correlation between the BET measurements (including surface area) and the high acute toxicity of some of the NPs. Whilst low toxicity, low solubility NPs have their effects via surface area (Duffin et al. 2007), the toxicity of the NPs in this panel was due to a number of factors other than simple surface area, as described above.

The work has shown that SAR based on chemometrics provides a plausible tool for describing factors that influence the toxicity of NPs. Because a panel of eighteen NPs is still considered to be too small, we were not able to develop a quantitative SAR model that can be applied to predict the toxicity of new nanoparticles. We believe that there are weaknesses in both the structural analysis of NP characteristics, as measured here, and the acute toxicity endpoints. In the case of the former we did not assess all structural parameters that have been suggested to be important in nanoparticle toxicity (Balbus et al. 2007; Fubini et al. 2010; Oberdorster et al. 2005b). However, we did address those parameters most obviously related to acute toxicity, including surface area, free radical generation and metal ion release. The fact that free radical generation was not simply related to acute toxicity reflects our findings with a panel of NP in previous studies (Lu et al. 2009), although it has been suggested to be an explanatory variable for toxicity of NP (Rushton et al. 2010). Possibly a greater weakness of the present study is the sole use of *in vitro* tests, which we have found not to effectively predict inflammation *in vivo,* apart from the haemolysis test (Lu et al. 2009) which, in our hands, is reasonably predictive of ability to cause inflammation. We reported here that the only NP causing haemolysis were (in order of potency) aminated polystyrene beads > nickel oxide > aluminum oxide. This is in agreement with our previous studies where aluminum oxide was inflammaogenic (Lu et al. 2009) whilst CeO_2 NPs are inflammogenic if well-dispersed (Cho et al. 2010); we have not yet instilled aminated polystyrene nanobeads *in vivo*, but we would predict that they too are inflammogenic.

There are a number of limitations to this work which are important to recognize, not only in the context of interpreting the current results but also in the field of nanotoxicity testing in general. First, NP characterization in the chemical context (e.g. SEM, sizing) might not accurately affect the characteristics of

the NPs, as found in cell culture experiments. For example, in the presence of physiologically important constituents (e.g. salts and proteins), NPs might undergo aggregation, or indeed, enhanced dispersal, such that the cells are presented with a particle surface area and chemistry that is very different from that predicted from measurements in dry powders or different media.

Second, the acute toxicity assays, by definition, only assess the immediate (24 h in this case) impact of NPs on hard end-points of cell death. This is only one overt facet of toxicity risk – it does not provide any information as to whether the exposure might lead to health problems driven by more subtle impacts that could manifest much later (e.g. chronic inflammatory conditions, atherosclerosis, cancer, infertility). Whilst the current study made some inroads into measurement of more subtle markers of cellular impacts that might ultimately alter function and induce health issues (e.g. changes in cell morphology, activation of NF-κB), the search for convenient *in vitro* tests to predict "toxicity" in its widest sense is a challenge for the field as a whole – the current study serves to reinforce this need. In other words, the toxicity hazard estimation should be combined with exposure studies in order to fully assess the potential risks. There are several other important challenges to relate physical properties to cytotoxicity (Rivera-Gil et al. 2012) that have not been fully taken into account in this work, such as coating of the inorganic core by a organic shell, as well as aggregation state.

Future research should continue to identify which structural parameters of NP should be determined in order to facilitate construction of a SAR for NP and the relevant endpoints should be measured and how they should be measured, and to standardise the process. The work in this paper is restricted to relatively simple NPs; more complex NPs, such as those with coatings, also deserve future study.

Acknowledgements

NERC are thanked for supporting this collaborative research project between the three institutions (grant reference: NE/E007791/1). The Leeds group also thanks EPSRC for supporting projects on engineering nanomaterials (EP/E040624/1 and EP/H008853/1). Thanks are also due to M. Sanchez-Sandoval Hohl, J-J. Sauvain, M. Riediker from Institute for Work and Health, Lausanne, Switzerland for performing the dithiothreitol (DTT) consumption test, Dr Tim Jones of University of Cardiff for measuring metals contents, and Mr. Fraiser-McNeil Watson of Malvern Instruments Ltd for useful discussions.

References

Arvizo RR, Miranda OR, Thompson MA, Pabelick CM, Bhattacharya R, Robertson JD, Rotello VM, Prakash YS, Mukherjee P. 2010a. Effect of Nanoparticle Surface Charge at the Plasma Membrane and Beyond. Nano Letters 10:2543-2548.

Arvizo RR, Mukherjee P, Prakash YS, Thompson MA, Miranda OR, Robertson JD, Rotello VM. 2010b. Surface charge determines functional interactions between nanoparticles and cells. Abstracts of Papers of the American Chemical Society 240.

Balbus JM, Maynard AD, Colvin VL, Castranova V, Daston GP, Denison RA, Dreher KL, Goering PL, Goldberg AM, Kulinowski KM, Monteiro-Riviere NA, Oberdorster G, Omenn GS, Pinkerton KE, Ramos KS, Rest KM, Sass JB, Silbergeld EK, Wong BA. 2007. Meeting report: Hazard assessment for nanoparticles - Report from an interdisciplinary workshop. Environmental Health Perspectives 115:1654-1659.

Balshaw DM, Philbert M, Suk WA. 2005. Research strategies for safety evaluation of nanomaterials, part III: Nanoscale technologies for assessing risk and improving public health. Toxicological Sciences 88:298-306.

Barlow PG, Donaldson K, MacCallum J, Clouter A, Stone V. 2005. Serum exposed to nanoparticle carbon black displays increased potential to induce macrophage migration. Toxicology Letters 155:397 - 401.

Barrett EP, Joyner LG, Halenda PP. 1951. The Determination of Pore Volume and Area Distributions in Porous Substances .1. Computations from Nitrogen Isotherms. Journal of the American Chemical Society 73:373-380.

Brunauer S, Emmett PH, Teller E. 1938. Adsorption of gases in multimolecular layers. Journal of the American Chemical Society 60:309-319.

Burello E, Worth A. 2011a. COMPUTATIONAL NANOTOXICOLOGY Predicting toxicity of nanoparticles. Nature Nanotechnology 6:138-139.

Burello E, Worth AP. 2011b. QSAR modeling of nanomaterials. WIREs Nanomedicine and nanotechnology 3:298-306.

Cho AK, Sioutas C, Miguel AH, Kumagai Y, Schmitz DA, Singh M, Eiguren-Fernandez A, Froines JR. 2005. Redox activity of airborne particulate matter at different sites in the Los Angeles Basin. Environmental Research 99:40-47.

Cho W-S, Duffin R, Poland CA, Duschl A, Oostingh GJ, MacNee W, Bradley M, Megson IL, Donaldson K. 2012. Differential pro-inflammatory effects of metal oxide nanoparticles and their soluble ions in vitro and in vivo; zinc and copper nanoparticles, but not their ions, recruit eosinophils to the lungs. Nanotoxicology 6:22-35.

Cho WS, Duffin R, Poland CA, Howie SEM, MacNee W, Bradley M, Megson IL, Donaldson K. 2010. Metal Oxide Nanoparticles Induce Unique Inflammatory Footprints in the Lung: Important Implications for Nanoparticle Testing. Environmental Health Perspectives 118:1699-1706.

Crane M, Handy RD, Garrod J, Owen R. 2008. Ecotoxicity test methods and environmental hazard assessment for engineered nanoparticles. Ecotoxicology 17:421-437.

Cui D, Tian F, Ozkan CS, Wang M, Gao H. 2005. Effect of single wall carbon nanotubes on human HEK293 cells. Toxicology Letters 155:73 - 85.

Donaldson K, Murphy FA, Duffin R, Poland CA. 2010. Asbestos, carbon nanotubes and the pleural mesothelium: a review of the hypothesis regarding the role of long fibre retention in the parietal pleura, inflammation and mesothelioma. Particle and Fibre Toxicology 7.

Donaldson K, Stone V, Tran CL, Kreyling W, Borm PJ. 2004. Nanotoxicology. Occupational and Environmental Medicine 61:727 - 728.

Duffin R, Tran L, Brown D, Stone V, Donaldson K. 2007. Proinflammogenic effects of low-toxicity and metal nanoparticles in vivo and in vitro: Highlighting the role of particle surface area and surface reactivity. Inhalation Toxicology 19:849-856.

Fubini B, Ghiazza M, Fenoglio I. 2010. Physico-chemical features of engineered nanoparticles relevant to their toxicity. Nanotoxicology 4:347-363.

Geller MD, Ntziachristos L, Mamakos A, Samaras Z, Schmitz DA, Froines JR, Sioutas C. 2006. Physicochemical and redox characteristics of particulate matter (PM) emitted from gasoline and diesel passenger cars. Atmospheric Environment 40:6988-7004.

Handy RD, Kammer Fvd, Lead JR, Hassellöv M, Owen R, Crane M. 2008. The ecotoxicology and chemistry of manufactured nanoparticles. Ecotoxicology 17:287-314.

Hornung V, Bauernfeind F, Halle A, Samstad EO, Kono H, Rock KL, Fitzgerald KA, Latz E. 2008. Silica crystals and aluminum salts activate the NALP3 inflammasome through phagosomal destabilization. Nature Immunology 9:847-856.

Jones T, Moreno T, BeruBe K, Richards R. 2006. The physicochemical characterisation of microscopic airborne particles in south Wales: A review of the locations and methodologies. Science of the Total Environment 360:43-59.

Kent RD, Vikesland PJ. 2012. Controlled Evaluation of Silver Nanoparticle Dissolution Using Atomic Force Microscopy. Environmental Science & Technology 46:6977-6984.

Lam CW, James JT, McCluskey R, Hunter RL. 2004. Pulmonary toxicity of single-wall carbon nanotubes in mice 7 and 90 days after intratracheal instillation. Toxicological Sciences 77:126 - 134.

Langmuir I. 1916. The constitution and fundamental properties of solids and liquids Part I Solids. Journal of the American Chemical Society 38:2221-2295.

Lu SL, Duffin R, Poland C, Daly P, Murphy F, Drost E, MacNee W, Stone V, Donaldson K. 2009. Efficacy of Simple Short-Term in Vitro Assays for Predicting the Potential of Metal Oxide Nanoparticles to Cause Pulmonary Inflammation. Environmental Health Perspectives 117:241-247.

Muller J, Huaux F, Lison D. 2006. Respiratory toxicity of carbon nanotubes: How worried should we be? Carbon 44:1048 - 1056.

Murdock RC, Braydich-Stolle L, Schrand AM, Schlager JJ, Hussain SM. 2008. Characterization of Nanomaterial Dispersion in Solution Prior to In Vitro Exposure Using Dynamic Light Scattering Technique. Toxicological Sciences 101:239-253.

Murphy F, Duffin R, Poland CA, Duffin R, Al-Jamal KT, Ali-Boucetta.H., Nunes A, Byene F, Prina-Mello A, Li S, Mather SJ, Bianco A, Prato M, Macnee W, Wallace WA, Kostarelos K, Donaldson K. Length dependent retention of carbon nanotubes in the pleural space of mice initiates sustained inflammation and progressive fibrosis on the parietal pleura. In press, ed.

Nel A, Xia T, Madler L, Li N. 2006. Toxic potential of materials at the nanolevel. Science 311:622-627.

Nel AE, Madler L, Velegol D, Xia T, Hoek EMV, Somasundaran P, Klaessig F, Castranova V, Thompson M. 2009. Understanding biophysicochemical interactions at the nano-bio interface. Nature Materials 8:543-557.

Oberdorster G, Maynard A, Donaldson K, Castranova V, Fitzpatrick J, Ausman K, Carter J, Karn B, Kreyling W, Lai D, Olin S, Monteiro-Riviere N, Warheit D, Yang H, Group ArftIRFRSINTSW. 2005a. Principles for characterizing the potential human health effects from exposure to nanomaterials: elements of a screening strategy. Part Fibre Toxicol 2:8.

Oberdorster G, Maynard A, Donaldson K, Castranova V, Fitzpatrick J, Ausman K, Carter J, Karn B, Kreyling W, Lai D, Olin S, Monteiro-Riviere N, Warheit D, Yang H, Group IRFRSINTSW. 2005b. Principles for characterizing the potential human health effects from exposure to nanomaterials: elements of a screening strategy. Part Fibre Toxicol 2:8.

Oberdorster G, Oberdorster E, Oberdorster J. 2005c. Nanotoxicology: an emerging discipline evolving from studies of ultrafine particles. Environmental Health Perspectives 113:823 - 839.

Poland C, Byrne F, Cho WS, Prina-Mello A, Murphy F, Davies GL, Volkov Y, Coey JM, Gounko Y, Duffin R, Donaldson K. Length –dependent Inflammatory and fibrogenic effects of nickel oxide nanowires in the lungs and the peritoneal cavity.

Poland CA, Duffin R, Kinloch I, Maynard A, Wallace WAH, Seaton A, Stone V, Brown S, MacNee W, Donaldson K. 2008. Carbon nanotubes introduced into the abdominal cavity of mice show asbestos-like pathogenicity in a pilot study. Nature Nanotechnology 3:423-428.

Powers KW, Brown SC, Krishna VB, Wasdo SC, Moudgil BM, Roberts SM. 2006. Research Strategies for Safety Evaluation of Nanomaterials. Part VI. Characterization of Nanoscale Particles for Toxicological Evaluation. Toxicological Sciences 90:296-303.

Powers KW, Palazuelos M, Moudgil BM, Roberts SM. 2007. Characterization of the size, shape, and state of dispersion of nanoparticles for toxicological studies. Nanotoxicology 1:42 - 51.

Price H, Arthur R, Sexton K, Gregory C, Hoogendoorn B, Matthews I, Jones T, BeruBe K. 2010. AIRBORNE PARTICLES IN SWANSEA, UK: THEIR COLLECTION AND CHARACTERIZATION. Journal of Toxicology and Environmental Health-Part a-Current Issues 73:355-367.

Puzyn T, Rasulev B, Gajewicz A, Hu X, Dasari TP, Michalkova A, Hwang H-M, Toropov A, Leszczynska D, Leszczynski J. 2011. Using nano-QSAR to predict the cytotoxicity of metal oxide nanoparticles. Nature Nanotechnology 6:175-178.

Rivera-Gil P, Aberasturi DJD, Wulf V, Pelaz B, Pino PD, Zhao Y, Fuente JMDL, Larramendi IRD, Rojo T, Liang X-J, Parak WJ. 2012. The Challenge To Relate the Physicochemical Properties of Colloidal Nanoparticles to Their Cytotoxicity. Accounts of Chemical Research DOI: 10.1021/ar300039j.

Rushton EK, Jiang J, Leonard SS, Eberly S, Castranova V, Biswas P, Elder A, Han XL, Gelein R, Finkelstein J, Oberdorster G. 2010. Concept of Assessing Nanoparticle Hazards Considering Nanoparticle Dosemetric and Chemical/Biological Response Metrics. Journal of Toxicology and Environmental Health-Part a-Current Issues 73:445-461.

Sauvain JJ, Deslarzes S, Riediker M. 2008. Nanoparticle reactivity toward dithiothreitol. Nanotoxicology 2:121-129.

Shvedova AA, Castranova V, Kisin ER, Schwegler-Berry D, Murray AR, Gandelsman VZ. 2003. Exposure to carbon nanotube material: assessment of nanotube cytotoxicity using human keratinocyte cells. Journal of Toxicology and Environmental Health-part A 66:1909 - 1926.

Thomas K, Sayre P. 2005. Research strategies for safety evaluation of nanomaterials, part I: Evaluating the human health implications of exposure to nanoscale materials. Toxicological Sciences 87:316-321.

Tsuji JS, Maynard AD, Howard PC, James JT, Lam CW, Warheit DB, Santamaria AB. 2006. Research strategies for safety evaluation of nanomaterials, part IV: Risk assessment of nanoparticles. Toxicological Sciences 89:42-50.

Valle S, Li WH, Qin SJ. 1999. Selection of the number of principal components: The variance of the reconstruction error criterion with a comparison to other methods. Industrial & Engineering Chemistry Research 38:4389-4401.

Verma A, Uzun O, Hu YH, Hu Y, Han HS, Watson N, Chen SL, Irvine DJ, Stellacci F. 2008. Surface-structure-regulated cell-membrane penetration by monolayer-protected nanoparticles. Nature Materials 7:588-595.

Table 1. The panel of 18 nanoparticles

Particles	Qualifier	Number	Supplier	Form
Carbon black	Printex 90	N1	Degussa	Dry
Diesel exhaust particles	EPA	N2	EPA	Dry
Nanotubes		N3	Vicki Stone	Dry
Fullerene		N4	Sigma	Dry
Polystrene latex	Unmodified	N5	Polysciences	Sus.
	Amine	N6	Sigma	Sus.
	Carboxylated	N7	Polysciences	Sus.
Aluminium oxide	7nm	N8	Krahn Chemie	Dry
	50nm	N9	AHT*	Dry
	300nm	N10	AHT*	Dry
Cerium oxide		N11	NAM**	Dry
Nickel oxide		N12	NAM**	Dry
Silicon oxide		N13	NAM**	Dry
Zinc oxide		N14	NAM**	Dry
Titanium dioxide	Rutile	N15	NAM**	Dry
	Anatase	N16	NAM**	Dry
Silver		N17	NAM**	Dry
		N18	NAM**	Sus.

* AHT: Allied High Tech, ** NAM: Nanostructure and Amorphous Material Inc

Table 2. The concentrations of various metals measured for the 18 nanoparticle samples

Particle names	Metal Concentration (µg/g)									
	Ti	V	Cr	Mn	Fe	Co	Ni	Cu	Zn	Cd
Carbon Black N1	0.000	0.057	0.000	0.305	0.000	0.002	0.263	1.161	9.687	0.008
Diesel Exhaust N2	2.320	0.312	16.47	20.81	208.4	0.508	4.940	2.235	3181	0.387
Nanotubes N3	0.000	0.100	0.000	0.161	13.10	0.000	0.299	0.123	0.460	0.001
Fullerene N4	0.000	0.084	0.000	0.000	0.000	0.000	0.534	0.142	4.837	0.000
Polystyrene Latex Unmodified N5	0.000	1.172	0.000	0.000	0.000	0.000	0.000	0.625	19.56	0.000
Polystyrene Latex Amine N6	4.368	0.779	0.343	0.199	0.000	0.006	0.440	18.23	58.71	0.010
Polystyrene Latex Carboxylated N7	0.000	1.018	0.000	0.000	0.000	0.000	0.000	2.588	22.323	0.000
Aluminuim Oxide N8	0.000	0.000	0.000	0.000	0.000	0.000	0.000	0.714	0.000	0.000
Aluminuim Oxide N9	0.000	0.031	0.000	0.000	0.000	0.000	0.056	0.099	4.987	0.000
Aluminuim Oxide N10	0.000	0.062	0.000	0.000	0.000	0.000	0.023	0.088	0.000	0.000
Cerium Oxide 7nm N11	0.000	0.004	1.058	0.128	0.000	0.000	0.616	0.191	112.9	0.007
Nickel Oxide 50nm N12	0.000	0.056	0.000	0.000	0.000	0.042	16963	0.286	0.000	0.038
Silicon Oxide 300nm N13	0.000	0.088	0.000	0.000	0.000	0.000	14.163	0.106	0.000	0.000
Zinc Oxide N14	0.000	0.096	0.000	0.000	0.000	0.000	1.336	0.047	8185	9.711
Titanium Dioxide Rutile N15	0.000	0.083	0.000	0.000	0.000	0.000	0.286	0.276	39.623	0.000
Titanium Dioxide Anatase N16	0.000	0.104	0.000	0.160	0.000	0.006	0.692	0.303	402.3	0.000
Silver N17	0.000	0.111	0.000	0.503	0.000	0.000	0.475	0.597	17.867	0.019
Silver N18	0.000	0.096	0.000	0.256	0.000	0.059	0.561	162.8	194.8	0.037

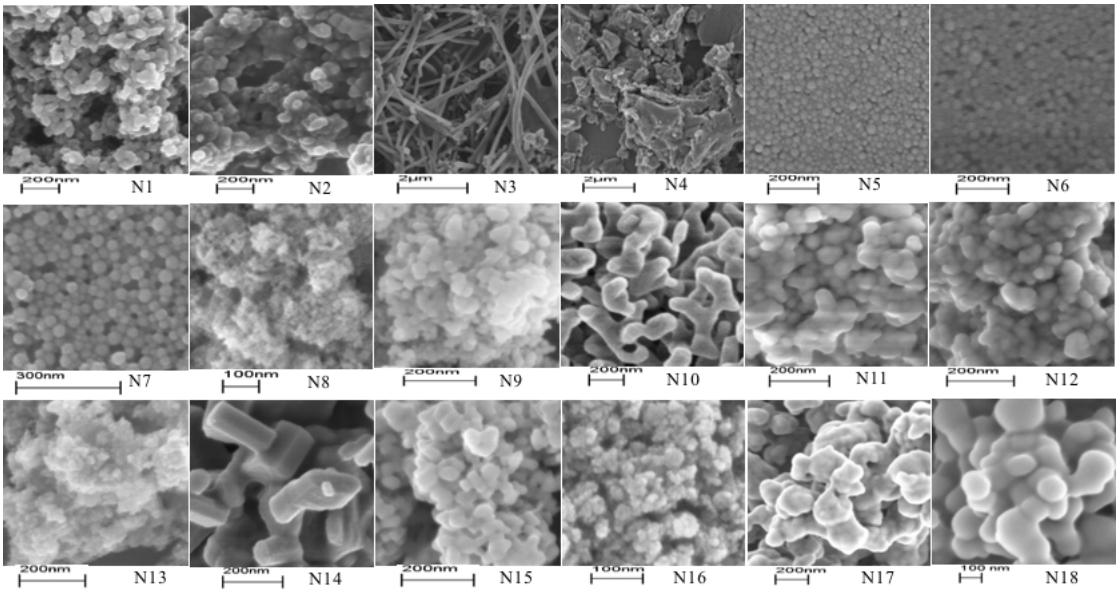

Figure 1. SEM images of the 18 nanoparticle samples

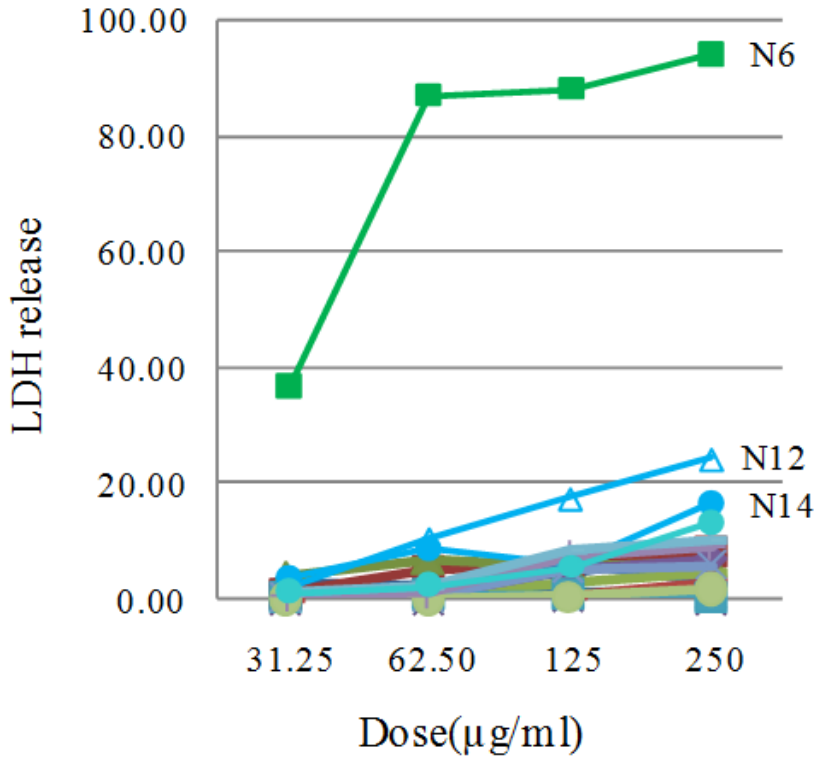
100.00
80.00
60.00
40.00
20.00
0.00
LDH release
N6
N12
N14
31.25
62.50
125
250
Dose(µg/ml)

(a)

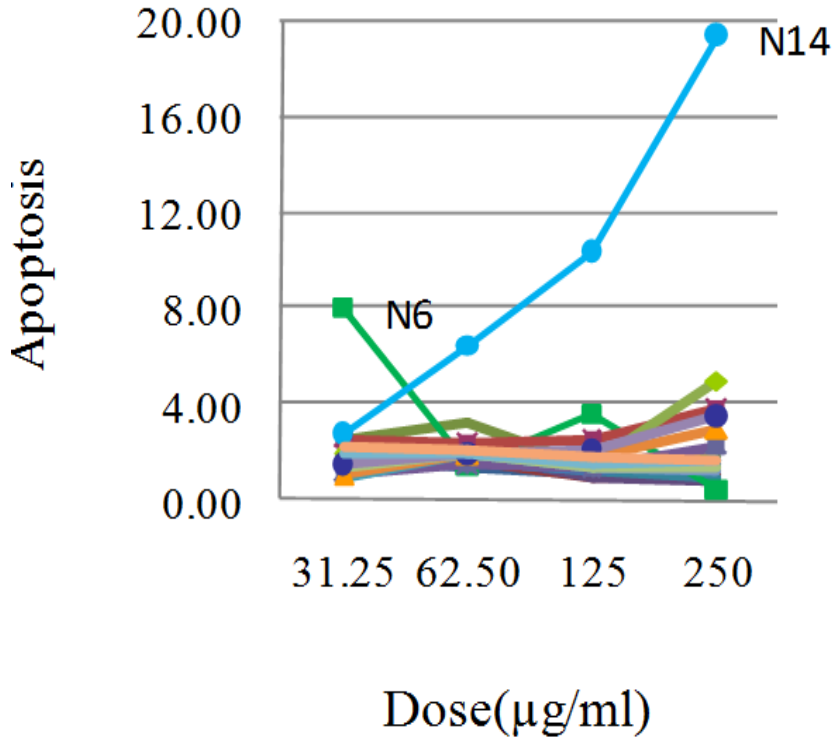
20.00
16.00
12.00
8.00
4.00
0.00
Apoptosis
N14
N6
31.25
62.50
125
250
Dose(µg/ml)

(b)

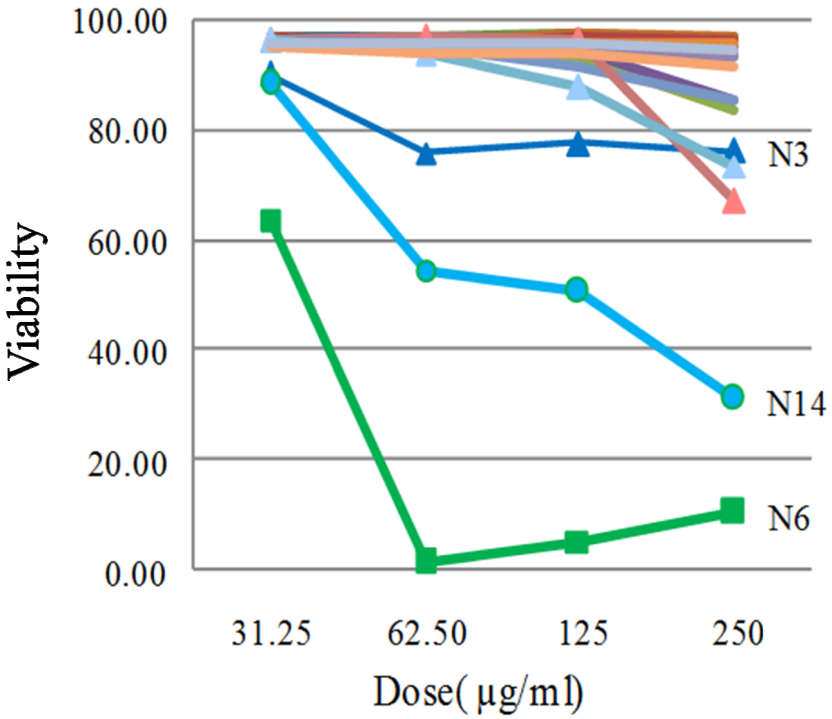

(c)

(d)

Figure 2. Cytotoxicity characterization. (a) Lactate Dehydrogenase Release (LDH), (b) apoptosis, (c) viability, and (d) necrosis

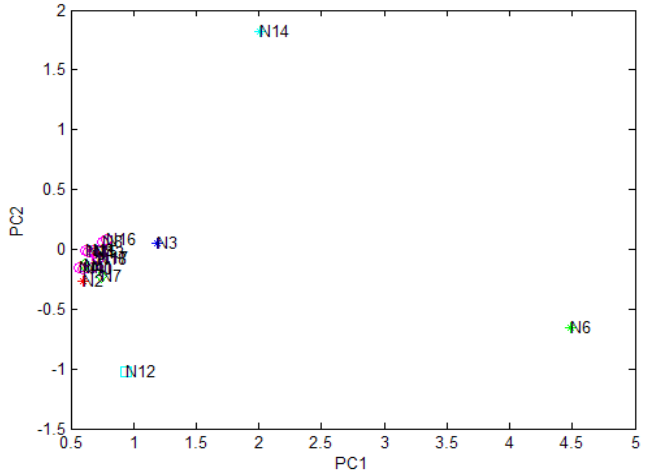

Figure 3. Plot of the first and second principal components based on principal component analysis of cytotoxicity data

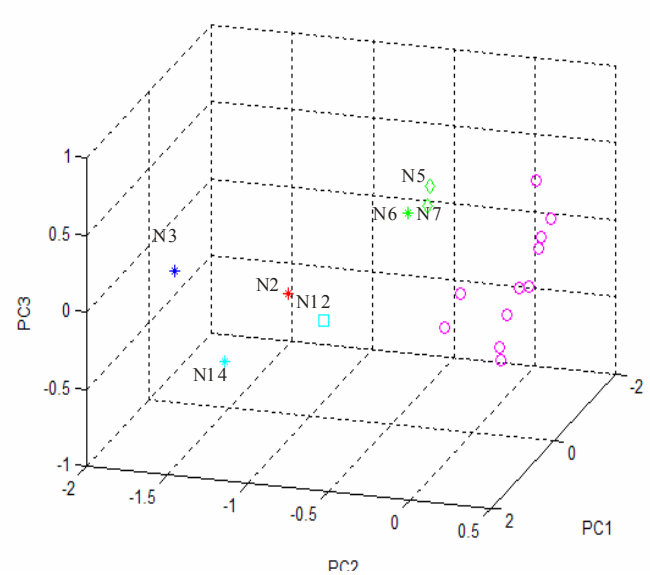

Figure 4. Principal component analysis of the structural and compositional descriptors for the panel of 18 nanoparticles (excluding BET and DTT measured descriptors since they are not available for the four wet samples).

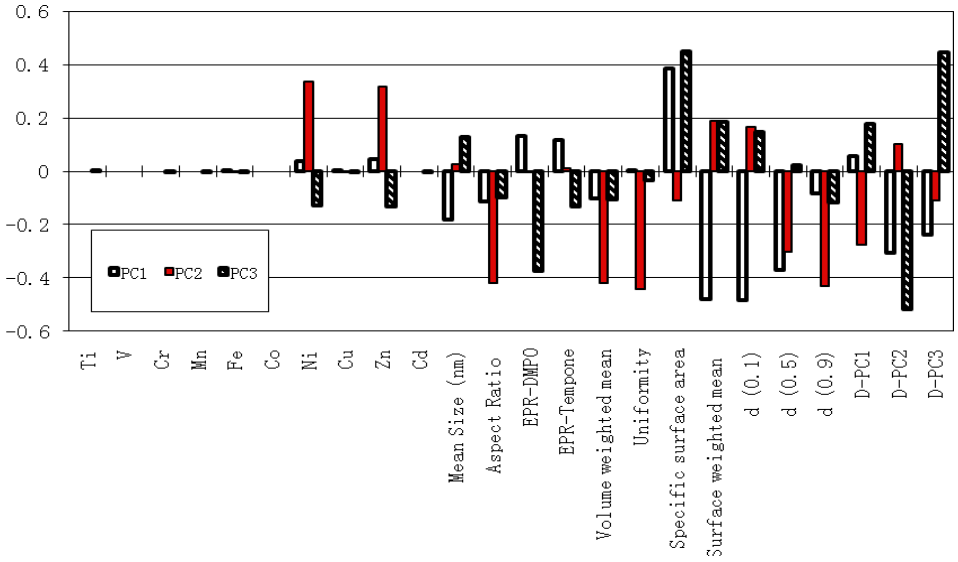

Figure 5. PC1, PC2 and PC3 Contribution plots based on principal component analysis of the structural and compositional descriptors for the panel of 18 nanoparticles (excluding BET and DTT measured descriptor since they are not available for the four wet samples)

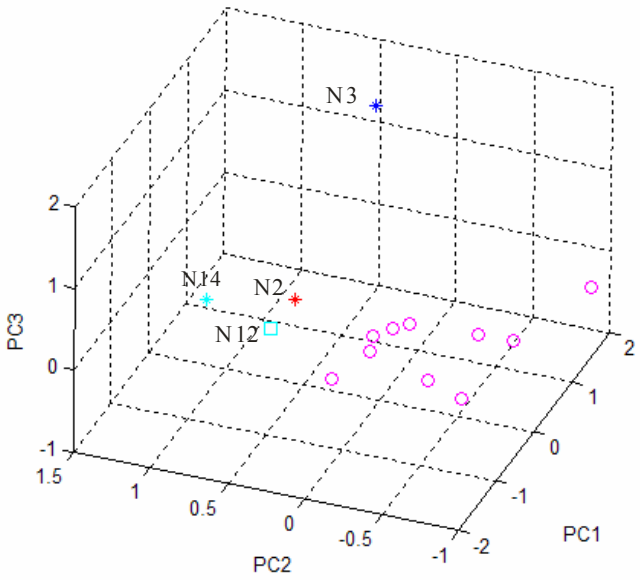

Figure 6 . Principal component analysis of the structural and compositional descriptors (all such descriptors including BET and DTT measurements) for the 14 dry nanoparticles.

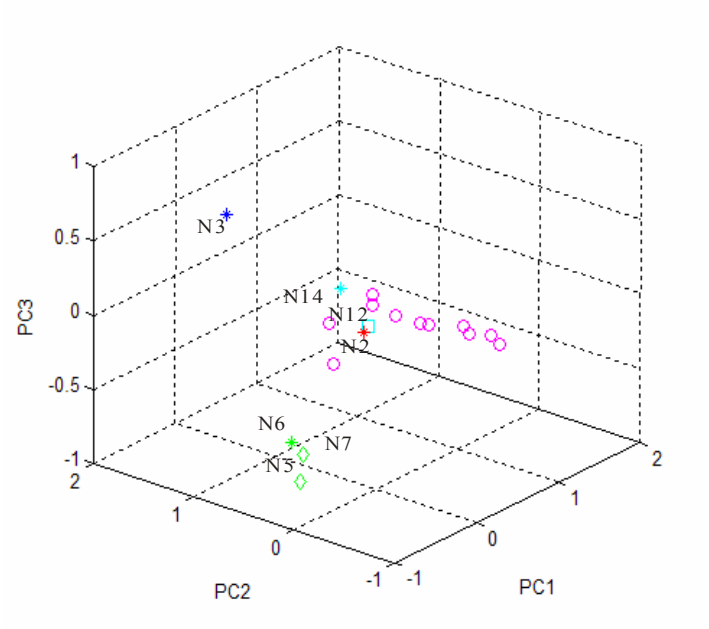

Figure 7 . Principal component analysis of the structural descriptors only for the panel of 18 nanoparticles (excluding BET and DTT measured descriptor since they are not available for the four wet samples, and metal contents)

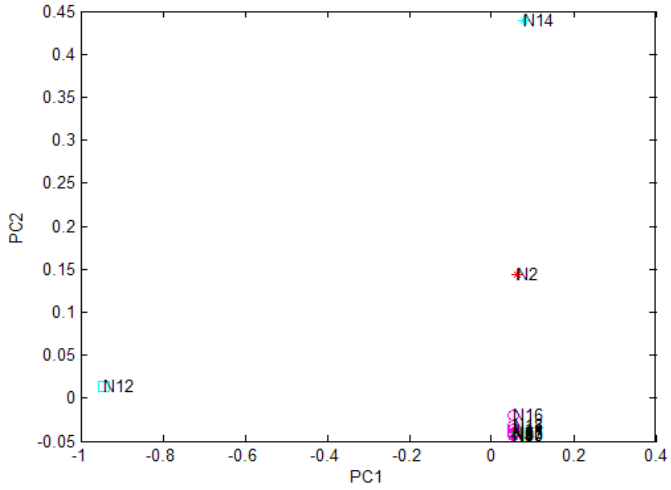

(a)

Figure 8. PC1-PC2 diagram from principal component analysis of the compositional descriptors only for the panel of 18 nanoparticles

Supplementary Materials

Table SM1 BET measurements by TriStar 3000

Surface Area (m^2/g)	Pore Volume (cm^3/g)	Pore Sizes (Å)
• Single point surface area at P/Po = 0.197 • BET Surface Area • Langmuir Surface Area • BJH Adsorption cumulative surface area of pores between 17.000 Å and 3000.000 Å diameter • BJH Desorption cumulative surface area of pores between 17.000 Å and 3000.000 Å diameter	• Single point adsorption total pore volume of pores at P/Po = 0.98 • BJH Adsorption cumulative volume of pores between 17.000 Å and 3000.000 Å diameter • BJH Desorption cumulative volume of pores between 17.000 Å and 3000.000 Å diameter	• Adsorption average pore width • BJH Adsorption average pore diameter • BJH Desorption average pore diameter • Mean size calculated from BET surface area • Particle density

Table SM2 Particle size and size distribution attributes measured by Mastersizer 2000

D[4,3] – the volume weighted mean or mass moment mean diameter
Uniformity - a measure of the absolute deviation from the median
Specific surface area - the total area of the particles divided by the total weight
D[3,2] – the Surface weighted mean or surface area moment mean diameter
D(v,0.5) – the size in microns at which 50% of the sample is smaller and 50% is larger. This value is also known as the mass median diameter or the median of the volume distribution
D(v,0.1) – the size of particle below which 10% of the sample lies
D(v,0.9) – the size of particle below which 90% of the sample lies
Size distribution - represented by 100 values, of which 16 values were found always zero for all samples, so each size distribution contains 84 values. Principal component analysis was used to reduce the 100 values to three principal components. In other words, the size distribution for each sample is represented by three attributes D-pc1, D_pc2 and D_pc3.

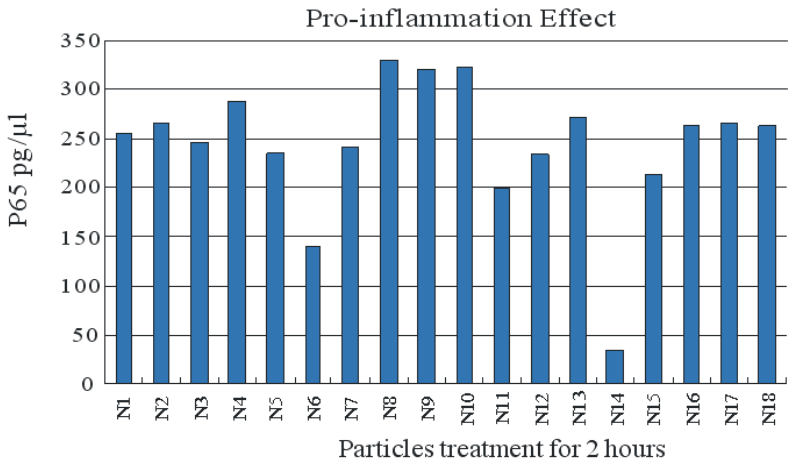

(a)

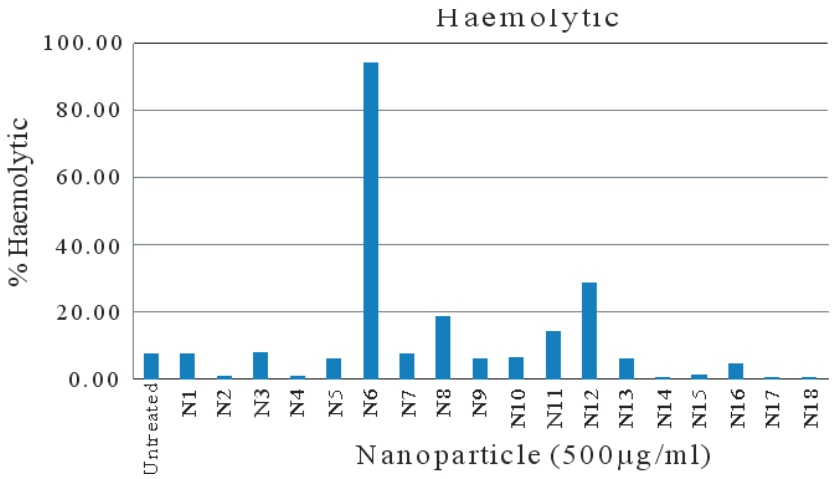

(b)

Figure SM1 . (a) Pro-inflammation effects by measuring P65 NF-kB protein in the nucleus following 2 hours exposure to the panel of 18 nanoparticles; (b) Cytotoxicity measured by Haemolysis

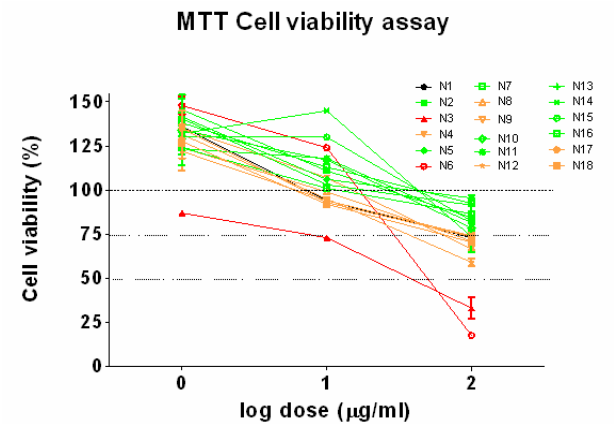

(a)

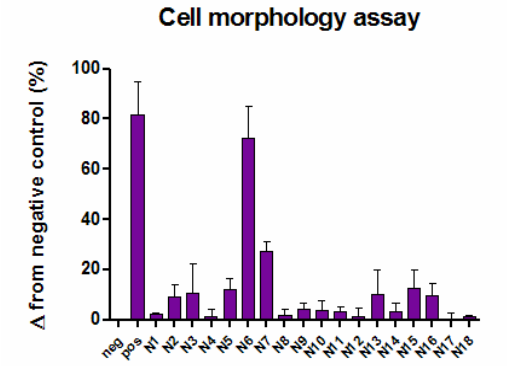

(b)

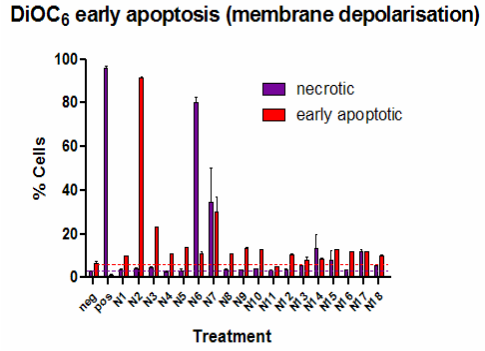

(c)

Figure SM2. (a)Dosimetric effect of the panel of nanoparticles (24 h exposure) on A549 cell viability, as assessed by the MTT assay. Japanese Nanotubes (N3) and Aminated beads (N6) were the only particles that were detected as having a highly cytotoxic effect using this assay (>50% loss of viability with 100 g/ml treatment). (b) Effect of nanoparticulate treatment (100 µg /ml; 24 h) on cell morphology (i.e. % cells with rounded appearance as opposed to “spread”; positive control: 100 µM H2O2). (c) Effect of nanoparticulate treatment (100 µg /ml; 24 h) on mitochondrial membrane depolarisation (early apoptosis) and propidium iodide (necrosis).